Atmospheric
Chemistry
and Physics

Rapid increases in ozone concentrations over the Tibetan Plateau caused by local and non-local factors

Chenghao Xu[1], Jintai Lin[1,2], Hao Kong[1], Junli Jin[3], Lulu Chen[4], and Xiaobin Xu[5]

[1]Laboratory for Climate and Ocean–Atmosphere Studies, Department of Atmospheric and Oceanic Sciences, School of Physics, Peking University, Beijing, 100871, China
[2]Institute of Carbon Neutrality, Peking University, Beijing, 100871, China
[3]Meteorological Observation Center of China Meteorological Administration, Beijing, 100081, China
[4]College of Urban and Environmental Sciences, Peking University, Beijing, 100871, China
[5]Key Laboratory for Atmospheric Chemistry, Institute of Atmospheric Composition, Chinese Academy of Meteorological Sciences, Beijing, 100081, China

Correspondence: Jintai Lin (linjt@pku.edu.cn)

Abstract. Changes in tropospheric ozone over the Tibetan Plateau (TP) profoundly affect the local ecosystems and human health. Yet previous studies on the TP ozone have focused on the background regions, with much less attention to the urban ozone. Here we quantify the ozone trends over the whole TP from 2015 to 2019 in the context of its long-term trends, with a focus on urban ozone. For this purpose, we use ozone measurements from 30 urban stations in 17 cities from the Ministry of Ecology and Environment (MEE) of China, the Waliguan baseline station, and four satellite products of tropospheric ozone. We further analyze the drivers of ozone trends through a combination of chemical transport model simulations, back-trajectory calculations, a bottom-up emission inventory, and a recent satellite-derived emission dataset of nitrogen oxides (NO_x). We find a strong increase in deseasonalized urban ozone at the MEE stations from 2015 to 2019 (by $1.71\,\mathrm{ppb\,yr^{-1}}$), which continues after the COVID-19 shock in 2020. The urban ozone trend far exceeds the trend at Waliguan (by $0.26\,\mathrm{ppb\,yr^{-1}}$) and the TP average trend (by up to $0.08\,\mathrm{ppb\,yr^{-1}}$) derived from the four satellite products. Interannual variations in meteorology do not produce significant ozone trends over the TP. Non-local factors contribute to the urban ozone growth, due to increased anthropogenic emissions in non-local source regions and changes in transport pathways. Another important contributor to the urban ozone growth is the 31.4 % increase in local anthropogenic NO_x emissions. Emission reductions in both the local and non-local source regions can help mitigate the rapid urban ozone growth over the plateau.

1 Introduction

Tropospheric ozone (O_3) is an important pollutant affecting human and ecosystem health (WHO, 2013; Desqueyroux et al., 2002; Mauzerall and Wang, 2001). Ozone is also a potent greenhouse gas and the main source of the hydroxyl radical (OH, the leading atmospheric oxidant) (Wang et al., 2019; Warneck, 1999). In recent years, surface ozone over eastern and southern China, such as in Beijing–Tianjin–Hebei, the Yangtze River Delta, and the Pearl River Delta, has shown rapid increases. Numerous studies have analyzed the roles

of local human activities, chemistry, meteorology, and atmospheric transport in the exacerbation of ozone pollution over these regions (Li et al., 2021a; Liu et al., 2023; Tan et al., 2023).

The Tibetan Plateau (TP; 27–45° N, 70–105° E; Fig. 1), located in southwestern China, covers about $2.5 \times 10^6\,\mathrm{km^2}$ and has an average altitude of more than 4000 m. Most of the Chinese part of the plateau is occupied by Qinghai Province in the north and Tibet Autonomous Region in the south. The TP consists mainly of natural wetlands and alpine forests, with

small populations and industries, which makes the region an important area to study Asian background ozone. Along with the recent economic development, the gross domestic product (GDP) of Qinghai and Tibet increased by 46 % and 63 % from 2015 to 2019 (National Bureau of Statistics of China, https://www.stats.gov.cn/, last access: 11 January 2025). Industrial and economic development may lead to increased emissions of ozone precursors such as NO_x (nitrogen oxides), and it has been shown that NO_x ozone production efficiency is higher at high altitudes, with the same amount of NO_x emitted potentially leading to more ozone production (Wang et al., 2018). Thus, the ozone changes over the TP urban areas are becoming increasingly important.

Previous studies on the TP ozone have mainly concentrated on a small number of background stations near the edges of the plateau, including Waliguan, Xianggelila, Nam Co, and Nepal Pyramid (Cristofanelli et al., 2010) or at very high altitude (Zhu et al., 2006). Only a few studies dealt with ozone at TP urban or suburban sites (Ran et al., 2014; Lin et al., 2015b; Chen et al., 2022b). Studies of surface ozone at Waliguan have shown significant growth over the last 2 decades (Xu et al., 2020), due to atmospheric transport and local emissions (Xu et al., 2016, 2018a). Transport plays an important role at these background stations, but the pollutant source areas are largely station dependent. Ozone at Waliguan in the northern TP is strongly influenced by air masses from northwestern and central China (Xue et al., 2011), and Xianggelila in the southeastern TP is mainly influenced by western China and Southeast Asia (Ma et al., 2014), while Nam Co is mainly affected by South Asia (Yin et al., 2017; Xu et al., 2018b). In addition, the Xianggelila and Nepal Pyramid stations are strongly influenced by the South Asian monsoon (Marinoni et al., 2013; Putero et al., 2014; Ma et al., 2014). Such spatial diversity in ozone sources means that more data are needed to study the ozone trends over the entire plateau.

In contrast, only a few studies have used data at the urban stations from the Ministry of Ecology and Environment (MEE) to analyze the TP ozone characteristics. Chen et al. (2022c) used a Geodetector analysis to find that natural factors dominate the urban surface ozone variations over the TP, while ecological degradation and desertification might have contributed to the ozone growth. Yin et al. (2022) used a random forest model to estimate the contribution of meteorology to surface ozone changes at 12 MEE cities on the TP from 2015 to 2020. Using a variety of meteorological parameters (wind, temperature, pressure, etc.) as predictors, they found that meteorology contributes less than 5 % of the interannual variability of ozone at the MEE stations. Overall, the trends and drivers of the TP urban ozone remain understudied.

Several types of numerical methods exist to study the drivers of surface ozone changes, including chemical transport models (CTMs), back-trajectory models, statistical analysis, and machine learning. The CTMs can quantitatively separate the contributions of individual drivers, as have been widely used in the study of Chinese ozone pollution (Ni et al., 2018, 2024; Wang et al., 2024). The CTMs rely on emission inventories for source attribution and are subject to large emission uncertainty for the TP. Chen et al. (2022a) simulated several air pollutants in the TP using WRF-Chem and found substantial underestimation in the modeled pollutant concentrations. They hypothesized that the emission inventory underestimates pollutant emissions on the TP by an order of magnitude. By comparison, the back-trajectory models analyze the transport pathways of air masses, as often used in the TP ozone studies (Chen et al., 2022b; Yang et al., 2022), but these models cannot quantitatively determine the exact locations of ozone formation and precursor emissions. Statistical and machine learning methods try to correlate ozone concentrations with multiple predicting variables (Weng et al., 2022; Xu et al., 2023; Zheng et al., 2023). For example, the random forest analysis by Yin et al. (2022) suggested the international variations of ozone at the TP MEE stations to be caused by anthropogenic influences, by only quantifying the meteorological impacts with no explicit analysis of atmospheric transport.

Here, we combine multiple observational datasets, emission data, and modeling approaches to assess the TP ozone trends and their drivers, with a particular focus on the urban areas where the MEE stations are located. We focus on the ozone trends over 2015–2019 in the context of its long-term changes. We use four satellite products of tropospheric ozone, urban ozone measurements at 30 MEE stations, and background ozone measurements at the Waliguan station to obtain comprehensive information on the ozone changes over the plateau. We then use the GEOS-Chem CTM, the HYS-PLIT back-trajectory model, the CEDS bottom-up emission inventory, and a satellite-based top-down emission dataset (PHLET-OMI) of NO_x to evaluate the roles of local contribution, non-local contribution, and meteorology in the ozone trends. Section 2 presents the ozone datasets, emission datasets, and the configurations of HYSPLIT and GEOS-Chem. Section 3 analyzes the ozone trends. Section 4 discusses the contributions of individual drivers. Section 5 summarizes the study.

2 Data and methods

2.1 Ground-based near-surface ozone data

Hourly concentrations of surface ozone are taken from the MEE website (http://www.cnemc.cn/en/, last access: on 21 April 2024). In 2013, a monitoring network for near-surface air pollutant concentrations was launched by the MEE (Li et al., 2019). So far, more than 1500 stations have been established, mostly in urban areas of China, providing hourly concentrations of six air pollutants: O_3, $PM_{2.5}$, PM_{10} (fine particulate matter smaller than 2.5 and 10 µm in aerodynamic diameter, respectively), NO_x, SO_2 (sulfur dioxide),
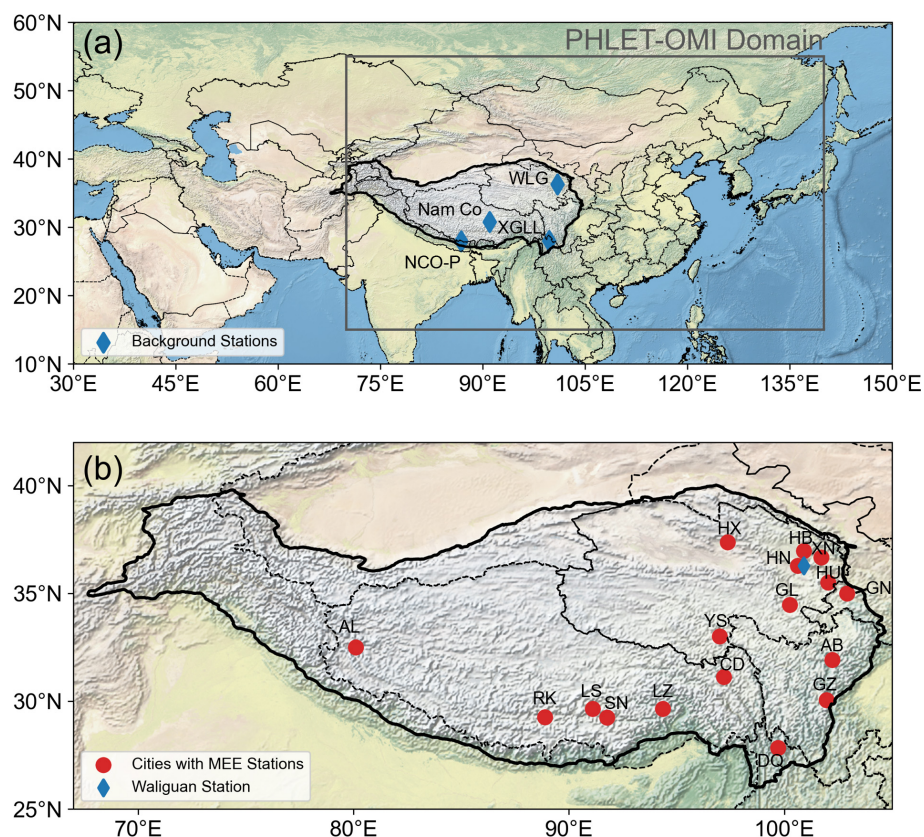
Figure 1. (a) The domain of PHLET-OMI NO_x emission data. The blue diamonds denote the background stations on the TP, including the Nepal Climate Observatory-Pyramid station (NCO-P), the Nam Co Comprehensive Observation and Research Station (Nam Co), the Mt. Waliguan Global Atmospheric Watch Station (WLG), and the Xianggelila Regional Atmosphere Background Station (XGLL). **(b)** Distribution of ground stations used in the study (made with Natural Earth), together with administrative (dashed line) and TP boundaries (solid line). The TP boundaries are downloaded from the Integration dataset of Tibet Plateau boundary (https://data.tpdc.ac.cn/zh-hans/data/61701a2b-31e5-41bf-b0a3-607c2a9bd3b3/, last access: 3 June 2024). The red dots denote the locations of the cities that have MEE stations: Aba (AB, 3 stations), Ali (AL, 1 station), Changdu (CD, 2 stations), Diqing (DQ, 1 station), Gannan (GN, 1 station), Ganzi (GZ, 1 station), Guoluo (GL, 1 station), Haibei (HB, 1 station), Hainan (HN, 1 station), Haixi (HX, 1 station), Huangnan (HU, 1 station), Lhasa (LS, 6 stations), Linzhi (LZ, 2 stations), Rikaze (RK, 2 stations), Shannan (SN, 2 stations), Xining (XN, 3 stations), and Yushu (YS, 1 station).

and CO (carbon monoxide). These measurement data have been widely used to study the changes and drivers of ozone pollution over central, eastern, and northern China (Liu and Wang, 2020b, a; Lu et al., 2020b; Li et al., 2021a; Pan et al., 2023; Wang et al., 2024). Between 2013 and 2015, a total of 37 air quality stations in 19 cities of the TP were added into the MEE network.

We apply the quality control method by Lu et al. (2018) to remove unreliable hourly data from the MEE stations, and use the method by Yan et al. (2018a) to obtain city-averaged, daily-averaged, and monthly-averaged ozone mixing ratios. First, stations with more than 30 % of hourly data missing during 2015–2019 are removed. For a given city, city-level hourly data are obtained by averaging all the selected stations in this city (Fig. 1b). Then we discard the days with more than 30 % of hourly data missing. Finally, we discard any months with valid data for less than 20 d. After quality

control, 30 stations in 17 cities are selected. Figure 1b shows the locations of these cities.

Ozone mixing ratios at the Waliguan station (36.28° N, 100.90° E) from 1994 to 2016 are obtained from the TOAR website (Tropospheric Ozone Assessment Report, https://igacproject.org/activities/TOAR, last access: 21 April 2024). Monthly average ozone mixing ratios at the Waliguan station from 2017 to 2019 are calculated by the Meteorological Observation Centre of the China Meteorological Administration. These data have been utilized extensively to study the background ozone (Xu et al., 2018a, 2020; Han et al., 2023; Ye et al., 2024). TOAR also includes the Xianggelila station (28.01° N, 99.44° E) and Nepal Pyramid station (27.95° N, 86.82° E) for hourly ozone concentrations. However, data from Xianggelila and Nepal Pyramid are only available through 2016 and 2014, respectively. In addition, these two stations are located on the southern edge of the TP and are significantly influenced by the South Asian monsoon

(Ma et al., 2014; Cristofanelli et al., 2010), making them difficult to represent the ozone characteristics over the vast area of the inner TP. There is also a Nam Co station in the south-central TP, but data from this station are not available. Thus, these three stations are not included in this study.

The ozone time series includes substantial seasonality due to seasonal variations in natural conditions and anthropogenic activities (Kalsoom et al., 2021). To uncover the ozone trend, we subtract the multi-year averaged seasonality from the monthly mean time series to obtain a deseasonalized dataset.

2.2 Satellite-based tropospheric ozone data

We use four satellite-based level-3 monthly tropospheric column ozone (TCO) products to analyze the tropospheric ozone changes over the entire TP. The first product is the OMI/MLS (Ozone Monitoring Instrument/Microwave Limb Sounder, https://acd-ext.gsfc.nasa.gov/Data_services/cloud_slice/new_data.html, last access: 21 April 2024). This product is calculated by subtracting the MLS stratospheric column ozone from the OMI total column ozone, with a horizontal resolution of $1°$ lat. $\times 1.25°$ long. covering the area from $60°$ S to $60°$ N. Data are available for the period since 2004. Ziemke et al. (2011) showed that the OMI/MLS data are in good correlation with ozonesonde measurements, with correlation coefficients ranging from 0.8 to 0.9 for the years 2005–2008 for WOUDC (World Ozone and Ultraviolet radiation Data Center) ozonesondes and 2004–2009 for SHADOZ (Southern Hemisphere Additional Ozonesondes) ozonesondes. The OMI/MLS TCO is lower than the ozonesonde data by about 1 ppb on average. OMI/MLS also shows good agreement with CTM simulation results (Ziemke et al., 2006; Yan et al., 2016). The second satellite product used here, OMI-RAL, is based on an optimal estimation method (OEM, Miles et al., 2015) and has been updated by the Copernicus Climate Change Service (C3S, https://cds.climate.copernicus.eu/cdsapp#!/dataset/satellite-ozone?tab=form, last access: 21 April 2024). In deriving OMI-RAL, the ozone vertical profiles from the ground to 450 hPa are produced based on the strongly variable ozone absorption at 280–320 nm. OMI-RAL spans October 2004 to the present with a horizontal resolution of $1° \times 1°$.

The third product, IASI-FORLI, provides global ozone column data from the surface to 6 km above sea level at $1° \times 1°$ from January 2008 to the present (https://cds.climate.copernicus.eu/cdsapp#!/dataset/satellite-ozone?tab=form, last access: 21 April 2024). The product is retrieved with the FORLI-O_3 OEM (Boynard et al., 2016). Boynard et al. (2018) showed that the IASI-FORLI tropospheric column is slightly higher than ozonesonde data in the high latitudes (by 4 %–5 %) and lower in the midlatitudes and tropics (by 11 %–13 % and 16 %–19 %, respectively). The fourth product, IASI-SOFRID, provides global tropospheric columns and profiles of ozone at $1° \times 1°$ from January 2008 to the present (https://thredds.sedoo.fr/iasi-sofrid-o3-co/, last access: 21 April 2024). The product is retrieved by SOFRID OEM, which is built based on the RTTOV (Radiative Transfer for TOVS) operational radiative transfer model (Matricardi et al., 2004). Good correlation (0.82) exists between IASI-SOFRID and ozonesonde data in 2008 in the midlatitudes (Dufour et al., 2012).

However, Boynard et al. (2018) found a negative drift in the IASI level-2 data, which leads to a negative drift of $-8.6 \pm 3.4 \%$ per decade in IASI-SOFRID for the Northern Hemisphere compared with the ozonesonde data. IASI-FORLI also shows a negative drift of -3.0% per decade for 0–60° N (Barret et al., 2020). Therefore, we correct the ISAI-SOFRID and IASI-FORLI ozone data by subtracting the drift trends above to the original ozone data.

For comparison with ground-based ozone measurements, tropospheric column ozone concentrations from the satellite products are converted to tropospheric mean mixing ratios. Following Ziemke et al. (2001), the concentration conversion employs the ideal gas equation of state, assuming hydrostatic equilibrium and constant gravity in the troposphere. Note that OMI/MLS and IASI-SOFRID ozone data represent the total tropospheric ozone column, OMI-RAL represents the ozone column from the ground to 450 hPa, and IASI-FORLI represents the ozone column from the ground to 6 km above sea level. As such, the converted ozone mixing ratios represent different vertical extents. In addition, all satellite data are deseasonalized prior to the trend analysis, as done for the ground-based ozone measurements.

2.3 Model simulations

We use the HYSPLIT (Hybrid Single-Particle Lagrangian Integrated Trajectory) model to calculate the back-trajectories of a large number of particles (Cohen et al., 2015) affecting Waliguan and the 17 cities with MEE measurements. To drive the model, we use the MERRA2 reanalysis data (Global Modeling and Assimilation Office (GMAO), 2015a, b, c, d). The MERRA2 data have a horizontal resolution of $0.5°$ lat. $\times 0.625°$ long. and 72 vertical levels, with each of the lowest 10 layers about 130 m thick. Particles are transported by the average winds and a turbulence transport component. The Kantha–Clayson scheme is adopted to compute the vertical turbulence (Kantha and Clayson, 2012). The HYSPLIT model has undergone extensive testing by comparing its simulations with actual measurements of atmospheric concentrations and deposition (Chai et al., 2015; Kim et al., 2020; Stein et al., 2015).

We calculate the back-trajectories to quantify the transport of anthropogenic pollutants, following previous work (Stohl, 2003; Cooper et al., 2010; Ding et al., 2013). For each city and Waliguan, an amount of 2000 particles is released from 100 m above the ground for each hour from 1 January 2015 to 31 December 2019, and the total run time for each parti-

cle is 192 h backward. In total, we conduct 1.6 billion back-trajectories for 17 cities and Waliguan in this study. The residence time distribution of the air mass is output as monthly averages on a $0.5° \times 0.5°$ grid. Then the "retroplume" is obtained with a unit of $s\,kg^{-1}\,m^3$, which represents the residence time of a simulated air mass divided by the air density. The residence time of the back-trajectory particles passing through the footprint layer (0 to 300 m above ground) can be multiplied by NO_x emissions (into the footprint layer, in units of $kg\,m^{-3}\,s^{-1}$) to calculate the quantity emitted into the retroplume (QNR, as mixing ratio) for NO_x. The QNR value for a given grid cell represents the amount of NO_x emitted into an air mass passing through its footprint layer, thus serving as a semi-quantitative indicator of ozone transport strength from emission source regions (Cooper et al., 2010; Stohl, 2003). The choice of the 192 h run time was obtained by considering both the previous work and the transport source region. In previous work, backward simulation run time were set from a few days to a few weeks (Cooper et al., 2010; Xu et al., 2018a; Yin et al., 2017), depending on the study area. Here we add 24 h of simulation time to the 168 h (7 d) setting of Xu et al. (2018a) for the Waliguan station on the TP, considering the possible variability of the urban stations on the TP, and finally determine a simulation duration of 192 h. Sensitivity experiments show that 192 h run time has resulted in a stabilization of the footprint layer residence time – the effect of increasing or decreasing the run time by 24 h on the calculated QNR is about $\pm 3\%$.

We further use the global GEOS-Chem CTM (v13.3.3; https://geoschem.github.io/, last access: 10 April 2024) to evaluate the role of meteorological changes from 2015 to 2019. The model is driven by MERRA2 at $2°$ lat. $\times 2.5°$ long., with 72 vertical layers. It computes the convective transport of chemicals from the archived MERRA2 convective mass fluxes (Wu et al., 2007). A non-local scheme for vertical mixing within the planetary boundary layer is implemented to account for different states of mixing based on the static instability (Lin and McElroy, 2010). For anthropogenic emissions, we use the MEIC (Multi-scale Emissions Inventory of China; http://www.meicmodel.org, last access: 12 August 2025) v1.4 inventory in China (Li et al., 2017; Zheng et al., 2018) and the CEDS (Community Emissions Data System v_2021_02_05) inventory in other regions (O'Rourke et al., 2021). For volatile organic compound (VOC) species not included in the MEIC, we also use the CEDS inventory. For soil NO_x, sea salt aerosols, and biogenic volatile organic compounds, we use an offline dataset at a horizontal resolution of $0.25°$ lat. $\times 0.3125°$ long. (Weng et al., 2020). The global GEOS-Chem model is run with anthropogenic emissions fixed at the 2015 levels while allowing the meteorology and meteorology-driven natural emissions to vary with time. The simulation period is from October 2014 to December 2019, with the first 3 months used for spin-up to reduce the effect of initial conditions.

Note that the QNR method does not account for the nonlinearity in ozone chemistry and the impact of VOC emission changes. Thus, its results should be interpreted as semiquantitative inference of ozone source contributions. On the other hand, although the CTM explicitly accounts for the effects of chemical nonlinearity and VOC emissions, it is subject to substantial challenges in simulating the TP urban ozone. First, there is no reliable VOC emission dataset for the TP and surrounding areas to allow a full exploration of the role of VOC in ozone growth. Existing bottom-up emission inventories do not or poorly account for local emission sources (e.g., combustion of cow dung and other biofuels used for cooking and/or heating and incense burning in religious activities) and emission factors, which has been confirmed in many studies (Cui et al., 2018; Lu et al., 2020a; Chen et al., 2022a; Tang et al., 2022; Li et al., 2023a, b), leading to large uncertainties in the calculated magnitude and spatial distribution of VOC emissions. Second, the local topography is complex in the TP (Kong et al., 2022), and the spatial scale of human activities on the TP is small and spatially dispersed, with the built-up area slightly larger than $100\,km^2$ in Xining and Lhasa and below $30\,km^2$ in other cities. Proper simulation of ozone chemistry in these cities requires a CTM resolution of 0.05–$0.1°$, for both meteorology and emissions, which poses a great challenge for current-generation CTMs in simulating the whole TP domain and surrounding areas (for local and non-local source attributions). Considering these limitations, we have elected to use the trajectory model and QNR results for ozone source analysis and further use nested GEOS-Chem CTM simulations to evaluate the impacts of simplification in the QNR method. The configuration of the nested GEOS-Chem model is shown in Sect. S1 in the Supplement.

2.4 Anthropogenic emission data for NO_x

In the TP region, the bottom-up anthropogenic emission inventories contain large uncertainties due to inaccuracy and inadequacy in human activity statistics and emission factors (Geng et al., 2017; Chen et al., 2022a). Thus, for the back-trajectory calculations, we use top-down NO_x emission data to reduce the effect of emission errors. The top-down NO_x emission data are an updated version of PHLET-OMI (Kong et al., 2022, 2019, 2025), which estimates June–August average NO_x emissions at $0.05° \times 0.05°$ in Asia (15–$55°$ N, 70–$140°$ E; Fig. 1a). PHLET-OMI is obtained by employing the POMINO-OMI satellite product for tropospheric NO_2 vertical column densities (VCDs) (Liu et al., 2019; Lin et al., 2015a, 2014) and the PHLET algorithm for emission retrieval. The PHLET emission data reveal considerable amounts of emission sources unaccounted for in existing bottom-up anthropogenic emission inventories (Kong et al., 2022) and natural emission parametrization (Kong et al., 2023). For example, the provincial total anthropogenic emissions of Tibet in PHLET are higher than current inventories

by 3 to 7 times (Kong et al., 2022); this result is confirmed by recent emission inference based on near-surface measurements (Zhang et al., 2025).

PHLET-OMI provides June–August average NO_x emissions in each year from 2012 to 2020. We remove the contributions of natural emission sources (soil and open fire) to focus on anthropogenic influences. We employ soil microbial emissions (Weng et al., 2020) and open fire emissions from the Global Fire Emissions Database (GFED4, https://www.globalfiredata.org/, last access: 8 December 2022; Giglio et al., 2013) that incorporate inter-annual variability (Kong et al., 2025).

To make use of the PHLET-OMI anthropogenic NO_x emissions within its spatial domain and account for the monthly variation in emissions, we first regrid the PHLET-OMI to match the CEDS, followed by a 3-year sliding average (the value for 2015 represents the average over 2014–2016, and so on) to minimize the effect of fluctuations in the number of valid satellite data and then combine PHLET-OMI with the monthly variation from the CEDS inventory (Eq. 1):

$$E_{r,g,y,m}^{\text{adjust}} = E_{r,g,y}^{\text{PHLET}} \frac{E_{r,g,y,m}^{\text{CEDS}}}{\sum_{m=6}^{8} n_m E_{r,g,y,m}^{\text{CEDS}} / \sum_{m=6}^{8} n_m}, \quad (1)$$

where r represents a region (a province in China or a country in the rest of Asia), g represents a grid cell within the region r, y represents a year, and m represents a month. n_m represents the number of days in the month m. For regions outside the PHLET-OMI domain, the CEDS inventory is used directly.

3 Elevated ozone concentrations

Figure 2 compares the monthly variation of deseasonalized ozone concentrations at Waliguan and 17 cities with MEE measurements. The MEE stations are located in the urban areas with local anthropogenic influences. In contrast, the Waliguan station is situated on the Waliguan Mountain with few local anthropogenic emissions, and thus its ozone concentrations are mainly influenced by the free troposphere, stratosphere, and global background ozone (Xu et al., 2018a, 2020). We use linear regression to derive ozone trends.

Deseasonalized ozone mixing ratios at Waliguan increase at a rate of 0.26 ppb yr^{-1} from 2015 to 2019 (Fig. 2a), which is consistent with the long-term trend from October 1994 to December 2019 (Fig. 2b). By comparison, deseasonalized ozone mixing ratios at the MEE stations averaged over 17 cities show much stronger growth (1.71 ppb yr^{-1}) during 2015–2019, suggesting potential influences from local human activities. The MEE ozone declines from 2019 to 2020, likely due to COVID-19, but it resumes rapid growth in the following years (by 1.89 ppb yr^{-1}) until the second half of 2023 (Fig. S1 in the Supplement). Note that 6 of the 30 sites showed a non-significant downward trend ($p > 0.05$). Lhasa

in the southern part of the TP had a total of six sites, three of which had negative linear trends (-0.04 to -0.09 ppb yr^{-1}, $p = 0.15$), which contributed to the non-significant increase in its urban mean ozone trend (0.46 ppb yr^{-1}, $p = 0.15$). Both of the two sites in Changdu in the central TP had negative linear trends (-0.10 to -0.50 ppb yr^{-1}, $p = 0.16$ to 0.71). Hainan in the northern TP also had a negative linear trend (-0.41 ppb yr^{-1}, $p = 0.15$). Overall, the trend of MEE ozone over 2015–2019 represents the growth during the most recent decade. This general growth is in contrast to the ozone changes over the North China Plain and Yangtze River Delta region, which show a rapid rise from 2013 to 2017 and a leveling off after 2017 (Liu et al., 2023). Such contrast likely reflects the regional differences in emission regulation and source areas. The central and eastern regions of China have had stringent emission reduction requirements, whereas the western regions are the most lenient in emission regulation (13th Five Year Plan, http://www.gov.cn/zhengce/content/2017-01/05/content_5156789.htm, last access: 11 January 2025). The regional difference in environmental regulation could also lead to more polluting factories moving to western China, making it more difficult to reduce emissions there (Cui et al., 2016; Zhao et al., 2017; Zheng and Shi, 2017). In addition, the TP ozone could be affected by pollution transport from surrounding Asian countries, which have experienced precursor emission growth in recent years (Abdul Jabbar et al., 2022; Bauwens et al., 2022).

To examine whether the TP ozone trends exhibit strong dependence on the time of day, we further explore the MEE measurements. The MEE ozone at different hours in the daytime shows similar strong growth from 2015 to 2019 (Fig. S2). Ozone increases at a rate of 2.15 ppb yr^{-1} in the early afternoon (local solar time (LST) 13:00, close to the overpass time of OMI), at a rate of 1.60 ppb yr^{-1} in the morning (09:00 LST, close to the overpass time of IASI), and at a rate of 1.86 ppb yr^{-1} for the maximum daily 8 h average (MDA8).

The TP is a vast area, and its ozone characteristics may vary considerably across the plateau (Yin et al., 2017). Therefore, we further examine four satellite products of tropospheric ozone to assess the ozone changes over the whole plateau (Fig. 3). Considering the drift in the IASI ozone data, we analyze the drift-corrected data (IASI-SOFRID_corr and IASI-FORLI_corr), with the original IASI data presented only for record.

From 2015 to 2019, OMI-RAL shows a strong ozone decline over 2015–2019 when averaged over the plateau, whereas other products suggest weak plateau-average ozone trends (within ± 0.3 ppb yr^{-1}) (Fig. 3). This is different from the long-term trends in these four products, which show growth over 2008–2019 (Fig. S3). Spatially (Fig. 4), OMI-RAL suggests strong ozone decline at most places but with sporadic positive trends. OMI/MLS, IASI-SOFRID_Corr, and IASI-FORLI_Corr suggest slight ozone decline over the southern plateau and growth over the
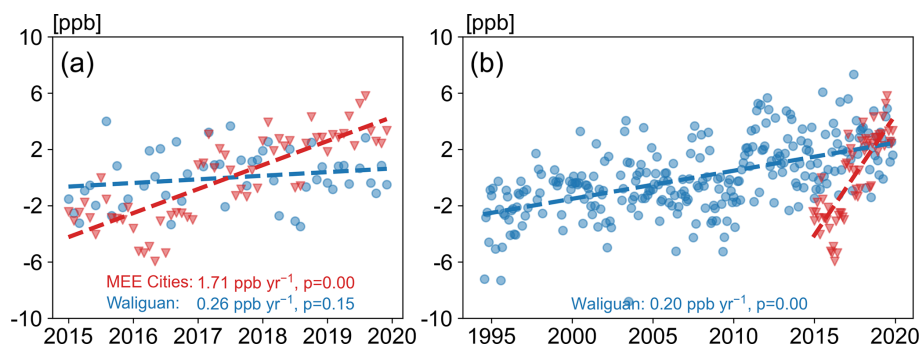
Figure 2. Monthly variation of deseasonalized ozone mixing ratios over the TP during **(a)** January 2015 to December 2019 and **(b)** August 1994 to December 2019 based on ground measurements. The results of MEE cities represent the mean of ozone mixing ratios in 17 cities. The data points represent deseasonalized ozone in individual months, and the dashed lines represent linear regression fit. The slope of linear regression and the p value are also shown.
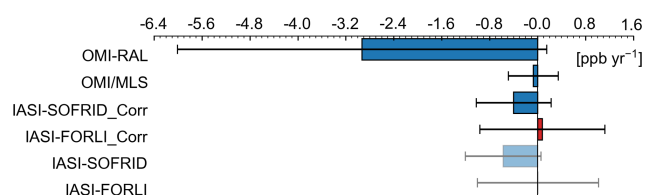

Figure 3. Trends of deseasonalized tropospheric ozone mixing ratios from 2015 to 2019 based on different satellite datasets. The error bar represents the standard deviation of all gridded data over the TP. The "_Corr" suffix means that the data have been corrected, as described in Sect. 2.3.

northern plateau, although the magnitudes of ozone trends are within $\pm 0.5\,\mathrm{ppb\,yr^{-1}}$. The spatial distributions of ozone trends over 2015–2019 are also different from the long-term growing trends over 2008–2019 in these four products (Fig. S4). The reasons for the inconsistent results of these satellite data are complex and may be related to their different observing equipments, different methods of inversion from radiance spectra to tropospheric ozone abundance, different retrieval altitudes, and different overpass times. Nevertheless, none of the satellite products shows ozone growth between 2015 and 2019 at a magnitude similar to that at the MEE stations.

In summary, the MEE data exhibit strong urban ozone growth from 2015 to 2019, in contrast to the much weaker ozone changes shown in the Waliguan background station and satellite datasets.

4 Drivers of ozone trends

Near-surface ozone concentrations are influenced by meteorological conditions and local emissions (Lu et al., 2019; Yan et al., 2018a, b). Over the TP, atmospheric transport of ozone and precursors from non-local source regions is also an important factor (Xu et al., 2016; Ma et al., 2014). In particular, regional transport from Asian countries has a strong influence on the tropospheric ozone over the plateau (Ni et al., 2018; Ma et al., 2022; Hu et al., 2024).

In this section, we analyze the individual contributions of three factors to the ozone changes over the TP, including meteorology, the non-local contributor, and the local contributor. For simplicity, we only analyze the drivers of trends in daily average ozone. Here, the "meteorology" represents the combined effect of meteorological changes (captured by global GEOS-Chem simulations at $2° $ lat. $\times 2.5°$ long.), meteorology-induced natural emission changes, and stratosphere–troposphere exchange that affects the global background ozone. The "non-local contributor" represents the combined effect of changes in precursor emissions and air mass transport pathway over the areas within 192 h of back-trajectory but outside the $1.5°$ latitude–longitude range of a receptor (the average location of MEE stations within a city or the location of Waliguan background station). The choice of the $1.5°$ range is made after considering the pixel size and data availability of OMI NO_2 product (Lin et al., 2015a; Zhang et al., 2022), which is used to derive PHLET-OMI NO_x emissions (Kong et al., 2019, 2022, 2023, 2025). The "local contributor" refers to the combined effect of anthropogenic emissions and transport pathway over the areas inside the $1.5°$ range of the receptor. The transport pathway affects the amount of residence time the air mass is situated in the footprint layers of high-emission regions.

4.1 Effect of meteorology

Figure 5 shows the effect of changes in meteorology on surface ozone over the TP during 2015–2019, as simulated by the global GEOS-Chem model at $2° $ lat. $\times 2.5°$ long. with fixed anthropogenic emissions but temporally varying meteorology. Over the plateau, ozone mixing ratios change little, except for the slight growth over the western and southeastern plateau and decline along the southern edge (Fig. 5b). The plateau-average rate of change is only about $-0.08 \pm 0.2\,\mathrm{ppb\,yr^{-1}}$. At the Waliguan station and
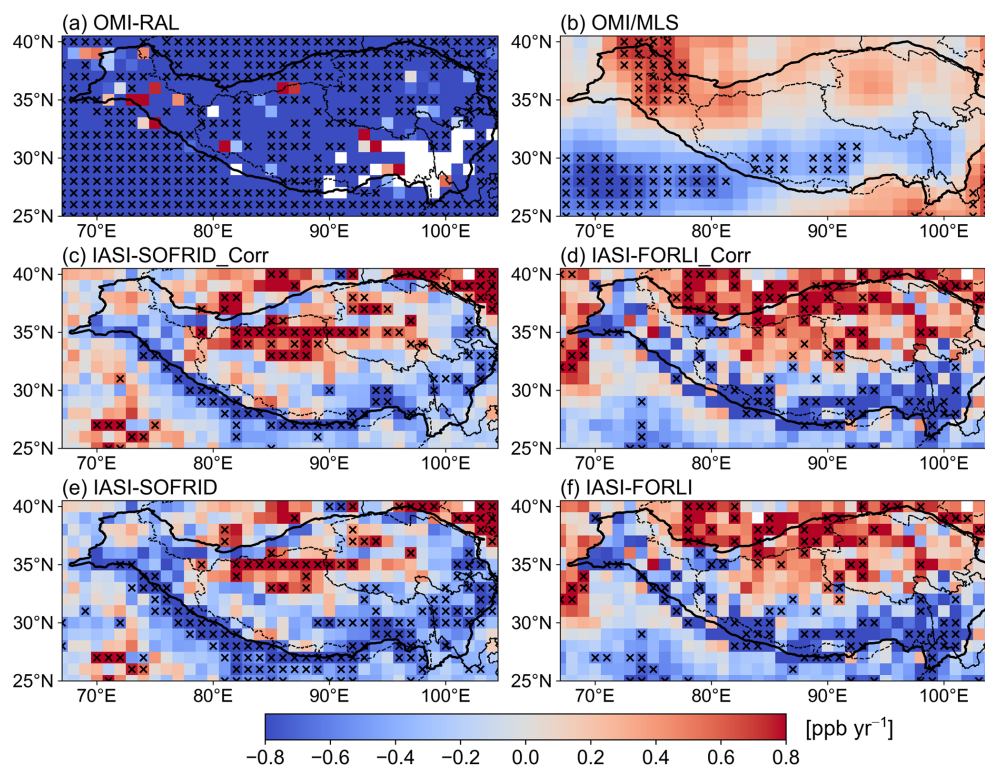
Figure 4. Spatial distribution of deseasonalized tropospheric ozone mixing ratio trends from 2015 to 2019 for **(a)** OMI-RAL, **(b)** OMI/MLS, **(c)** IASI-SOFRID_Corr, **(d)** IASI-FORLI_Corr, **(e)** IASI-SOFRID, and **(f)** IASI-FORLI. Each cross means the trend in that grid cell is statistically significant (p value < 0.05).

the 17 cities with MEE data, the rates of change are -0.15 and $-0.1 \pm 0.16\,\mathrm{ppb\,yr^{-1}}$, respectively. Thus, meteorology is not an important factor for the observed ozone growth of $1.71\,\mathrm{ppb\,yr^{-1}}$ at the MEE stations (Fig. 2). This result is consistent with previous work for 12 cities with MEE stations over the TP based on a random forest model (Yin et al., 2022).

4.2 Effect of non-local contributor

To evaluate the effect of non-local contributor, we use the HYSPLIT model to conduct 192 h back-trajectories for the 17 cities and Waliguan during 2015–2019. As shown in Fig. 6, air masses reaching the 17 TP cities with 192 h come from China and nearby countries. Most air masses reaching the 17 cities stay at the edge of the plateau for a long time because the air masses are blocked by the topography (e.g., the Himalayas). Among the source areas outside China, Nepal, Northeastern India, Myanmar, and Bangladesh exhibit longer residence time in the footprint layer (i.e., 0–300 m above the ground). Overall, there is little interannual variation in the spatial distribution of residence time. In 2018, there was an increase in residence time over the eastern part of China, likely due to more pronounced easterly winds in the lower troposphere on the eastern side of the plateau (not shown). Such a wind anomaly is associated with the subtropical high

anomaly in summer 2018 (Yuan et al., 2019; Ding et al., 2019). Summer is the high ozone season in eastern China, and the increased residence time of air masses from the east may lead to increased ozone transport.

To further understand the non-local contribution through transport, we calculate the non-local QNR by multiplying the residence time in the footprint layer of individual locations by their NO_x emissions and then summing this over those locations outside the 1.5° range of each receptor. From 2015 to 2019, the non-local QNR increases at a rate of $0.14\,\mathrm{ppb\,yr^{-1}}$ (p value $= 0.04$) (Fig. 7a). The QNR growth rate due to changes in transport pathway alone is about $0.07\,\mathrm{ppb\,yr^{-1}}$ (p value $= 0.20$), while emission changes alone result in a trend of $0.06\,\mathrm{ppb\,yr^{-1}}$ (p value $= 0.00$) (Fig. 7b–c). The non-local QNR is mainly driven by changes in South Asia (India, Bangladesh, etc.) and the central and western provinces of China (Gansu, Sichuan, etc.). Although the non-local emissions in Qinghai and Tibet are increasing (Fig. S5c), the absolute amount of emissions in these two regions is too low to dominate the non-local QNR. Emissions in Southeast Asia have not changed significantly in recent years, and the short residence time of the air mass makes it not a major contributor to the non-local QNR changes. The upward trend of QNR is related to the peaks in 2017 and 2018, but the drivers of these two peaks are not completely the same. As
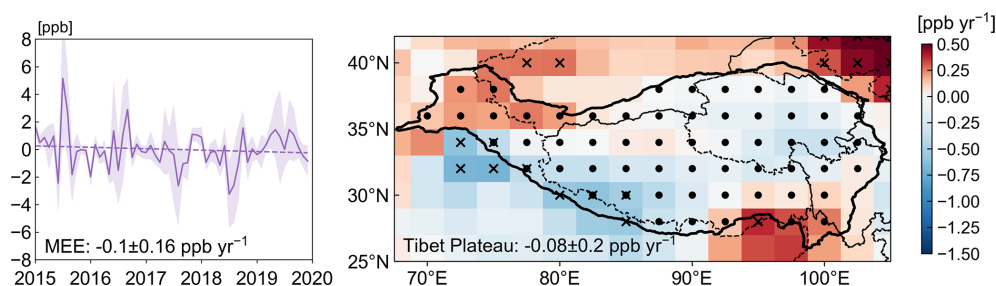
Figure 5. Changes in ozone mixing ratios due to changes in meteorology over 2015–2019 simulated by the global GEOS-Chem model. **(a)** Deseasonalized monthly mean ozone averaged over the 17 cities with MEE measurements. **(b)** Spatial distribution of deseasonalized ozone trends over the plateau. In **(b)**, the dots denote the grid cells belonging to the TP, and the crosses denote statistically significant ozone trends (p value < 0.05).
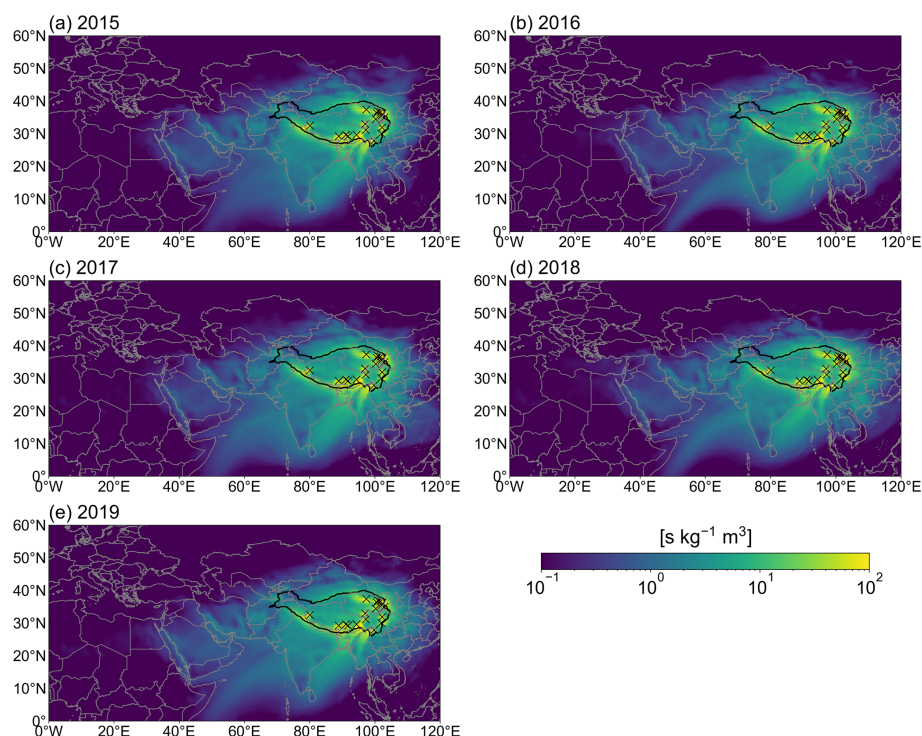

Figure 6. Distribution of the annual average residence time in the footprint layer for the 17 cities with MEE stations in **(a)** 2015, **(b)** 2016, **(c)** 2017, **(d)** 2018, and **(e)** 2019. The crosses denote the locations of 17 cities.

shown in Fig. S5, the 2017 QNR peak was more due to QNR growth in South Asia, such as India and Bangladesh. Although the total South Asian emissions peaked in 2018, in northern South Asia, closer to the TP, emissions peaked in 2017 (not shown), which could be a possible reason besides the change in transport pathway for the high QNR values seen in 2017 (Fig. S5c). The peak in the summer of 2018, instead, was caused more by the increase in QNR in Sichuan and other central regions of China. Emissions in China's central and western provinces have been declining in recent years (Fig. S5c). As mentioned above, the subtropical high pressure anomaly in the summer of 2018 caused the source of air mass transport to expand eastward and pass more through

the high-emission regions in central China, and this change in the transport path of the air mass is what dominated the emergence of the peak of QNR in 2018. As for 2015 and 2019, both emissions and transport pathway contribute to low QNR values.

The interannual variation of non-local QNR for the Waliguan background station is similar to that for the MEE stations, although with a stronger contribution from transport pathway and a weaker contribution from non-local emission changes (Fig. S6a–c). These results suggest a considerable positive contribution of regional transport to ozone growth over the whole plateau.
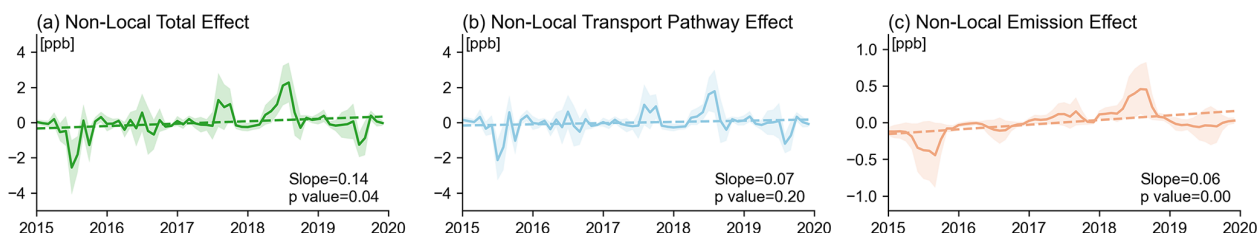
Figure 7. Deseasonalized monthly variation of non-local QNR averaged over the 17 cities. **(a)** Non-local QNR changes due to the combined effect of changes in anthropogenic emissions and in transport pathway. **(b)** Non-local QNR changes due to transport pathway alone. **(c)** Non-local QNR changes due to anthropogenic emissions alone. The shaded area represents the standard deviation of the data across 17 cities.

4.3 Effect of local contributor

To further delineate the contribution of changes in local air mass residence time and anthropogenic emissions, we analyze the local PHLET-OMI NO_x emissions and QNR within the $1.5°$ range of the 17 cities. The interannual variation of 3-year summer average local anthropogenic NO_x emissions shows a growth of 31.4% from $1.49\,\mathrm{t\,h^{-1}}$ in 2015 to $1.96\,\mathrm{t\,h^{-1}}$ in 2019 (Fig. 8a). This growth may be associated with multiple factors. Compared to 2015, possession of private vehicles in Qinghai and Tibet in 2019 increased by 58% and 79% respectively, the urban population rose by 16% and 26% respectively, and industrial GDP and electricity consumption also increased significantly (National Bureau of Statistics of China, https://www.stats.gov.cn/, last access: 11 January 2025). In addition, the relatively more lenient emission reduction targets (13th Five-Year Plan, http://www.gov.cn/zhengce/content/2017-01/05/content_5156789.htm, last access: 11 January 2025) in the provinces of Qinghai and Tibet may have led to relatively less stringent regulation, ultimately resulting in an upward trend in NO_x emissions. The TP is a remote region, and the ozone sensitivities of its urban areas are very different from those of cities in eastern China. Satellite formaldehyde (HCHO) and NO_2 ratio data show that the TP is largely in the NO_x-limited regime in 2019 (Li et al., 2021b). Lhasa, the capital city of the Tibet Autonomous Region, still had NO_x-limited sensitivity between 2016 and 2019 (Wang et al., 2021). Besides the rapid increase in NO_x emissions, an observational study suggests that the increase in VOC concentrations may be even more intense in the urban areas of the TP. In particular, Tang et al. (2022) found that concentrations of VOCs in urban areas of the TP increase to 2.5 times from 2012–2014 to 2020–2022 (mainly driven by a 3-fold increase in the concentrations of aromatic and alkane hydrocarbons), which may lead to greater sensitivity of ozone to NO_x emissions on the TP. This suggests an important contribution from local anthropogenic emissions in the elevated urban ozone over the TP.

Figure 8b further shows that for the 17 cities, the local contribution to QNR increases significantly from 2015 to 2019 with a trend of $0.06\,\mathrm{ppb\,yr^{-1}}$, with a total growth of
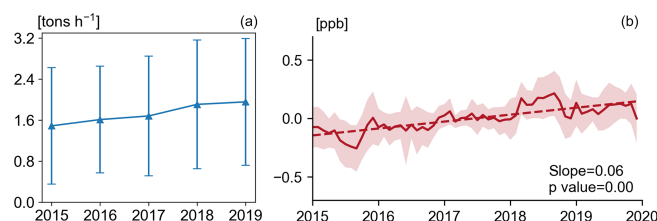

Figure 8. Changes in local anthropogenic emissions and QNR for within $1.5°$ of the 17 cities. **(a)** Time series of 3-year moving average PHLET-OMI NO_x anthropogenic emissions in summer. Here, the value for 2015 represents the average over 2014–2016, and so on. **(b)** Deseasonalized monthly variation of local QNR. The error bar in **(a)** and shaded area in **(b)** represent the standard deviation of data across 17 cities.

33.5% over these years. This trend is contributed mainly by the growth in local NO_x emissions (31.4%). It contrasts with the respective trend of local QNR for Waliguan ($-0.00\,\mathrm{ppb\,yr^{-1}}$) (Fig. S6d). The local QNR growth for the 17 cities ($0.06\,\mathrm{ppb\,yr^{-1}}$) is smaller than that for the non-local contribution ($0.14\,\mathrm{ppb\,yr^{-1}}$, Fig. 7a). We further analyzed the average QNR for the three cities with decreasing trends (Lhasa, Changdu and Hainan). As shown in Fig. S7, the trend of non-local contributions is slightly higher than the average of the other cities on the TP, while the local contributions show a weak decreasing trend ($-0.01\,\mathrm{ppb\,yr^{-1}}$). This decline combined with meteorological effects may have offset the non-local QNR trend, which resulted in the ozone not showing a significant increase in these regions. However, note that the QNR calculation does not consider the effect of distance from the emission source regions to the TP cities and the associated ozone loss (through chemical reactions and/or dry deposition) along the transport pathway. Taking the distance into account, each unit of ozone mass produced from more distant source regions might be lost more substantially and thus have a weaker effect on these cities. This means that the local contribution is indeed a major cause of ozone growth in the urban area over TP.

Given the limitations of the QNR method in not accounting for VOC emissions and chemical nonlinearity, we further conduct nested GEOS-Chem simulations for summer

(June, July, and August) 2015 and 2019 to compare with the QNR results. The model is driven by our updated anthropogenic NO_x emissions as well as rough adjustments of anthropogenic VOC emissions over the TP based on the current literature, including enhancement of VOC emissions upon the current inventories and emission growth in recent years (Sect. S1). To focus on the impact of chemistry, the meteorology is fixed at the 2015 level, but the anthropogenic emissions are adjusted in different model simulation scenarios (Table S1 in the Supplement). The GEOS-Chem results show that when changes of NO_x and VOC emissions were considered together, increases in local and non-local emissions from 2015 to 2019 increase the summertime ozone in the TP cities by comparable amounts (0.71 versus 1.21 ppb averaged over 17 cities), and inclusion of local and non-local emissions together leads to a larger ozone increase (1.52 ppb) (Table S2). Increases in NO_x emissions are the main driver of the simulated ozone growth – the ozone increase caused by NO_x emission increase alone is close to when both NO_x and VOC emission increases are taken into account (1.34 versus 1.52 ppb when local and non-local emission changes are considered together, and 1.02 versus 1.21 ppb when non-local emission changes are considered alone). These model results suggest that the ozone nonlinearity and the changes in anthropogenic VOC emissions have relatively small effects on the TP urban ozone growth studied here, and the use of QNR leads to reliable inference regarding the local and non-local drivers of TP ozone growth. Nevertheless, the nested GEOS-Chem simulations still underestimate the observed ozone growth in the TP cities, which is likely due to the lack of reliable high-resolution VOC emission information (including the simplicity in our VOC emission adjustments), the small spatial domain of TP cities, and the complex topography, as detailed in Sect. 2.3.

5 Conclusions

This study uses the ozone measurements from MEE, Waliguan, and satellite products to analyze the ozone changes over the TP. The ozone mixing ratios at the MEE stations in the urban areas increase significantly at a rate of $1.71 \, ppb \, yr^{-1}$ from 2015 to 2019, averaged over 17 cities. A similar rate of growth occurs after the plateau resumes from the COVID-19 shock in 2020. In contrast, ozone at Waliguan rises at a rate of $0.26 \, ppb \, yr^{-1}$ from 2015 to 2019, consistent with its long-term trend over 1994–2019. Additionally, tropospheric ozone over the TP does not suggest a strong upward trend from 2015 to 2019. These results suggest strong anthropogenic influences on ozone growth over the TP cities over the past decade.

We further quantify the contributions of three factors to the ozone growth at the cities using GEOS-Chem simulations, HYSPLIT calculations, the CEDS emission inventory, and the PHLET-OMI top-down emission dataset. These factors include meteorology, the local contributor, and the non-local contributor. As simulated by GEOS-Chem, the meteorological changes over the plateau do not result in near-surface ozone growth between 2015 and 2019, albeit with clear interannual variations. The meteorology-driven ozone trends over the whole TP and the 17 cities are only -0.10 ± 0.16 and $-0.08 \pm 0.20 \, ppb \, yr^{-1}$, respectively.

In contrast, the non-local QNR, calculated by combining the HYSPLIT modeling and NO_x emissions for the areas outside $1.5°$ range of each city, shows a growth rate of $0.14 \, ppb \, yr^{-1}$. The non-local QNR growth is driven by the changes in the transport pathway of air mass and the anthropogenic emission increases in non-local source regions. This likely suggests a substantial non-local contribution to the observed urban ozone growth over the TP, due to the rapid increase of anthropogenic emissions in the transport source regions and more frequent transport of air masses passing through non-local high-emission regions.

The local QNR for the 17 cities exhibits a growth of $0.06 \, ppb \, yr^{-1}$ (or 33.5 % in total) from 2015 and 2019, with the majority caused by the increase in local NO_x emissions (by 31.4 %). This is an indication of important contribution of local precursor emissions to the observed TP urban ozone growth. Considering the ozone loss during atmospheric transport at different distances, local and non-local contributions to the rapid rise in the TP urban ozone might be comparable.

Overall, our study suggests that the large rate of urban ozone growth over the TP cities during the recent decade is likely caused by a combination of increases in local anthropogenic emissions, non-local anthropogenic emissions, and more frequent transport passing through non-local high-emission regions. These local and non-local factors should be considered in future studies of ozone and its mitigation over the plateau.

It is important to note that the QNR does not consider the nonlinearity in ozone chemistry and VOC emissions, which may introduce uncertainty in ozone source attribution. Although the QNR results are supported by nested GEOS-Chem CTM simulations for summertime ozone, the CTM simulations themselves are subject to limitations in resolution and emission inputs. Future work should focus on obtaining reliable, high-resolution precursor emissions, especially for speciated VOC emissions. Combining the trajectory models, CTMs and statistical and/or artificial intelligence methods might allow for low-cost kilometer-resolution simulation of ozone chemistry and source inference to better quantify the individual and combined effects of various emission and meteorological factors on the TP urban ozone.

References

Abdul Jabbar, S., Tul Qadar, L., Ghafoor, S., Rasheed, L., Sarfraz, Z., Sarfraz, A., Sarfraz, M., Felix, M., and Cherrez-Ojeda, I.: Air Quality, Pollution and Sustainability Trends in South Asia: A Population-Based Study, Int. J. Env. Res. Pub. He., 19, 7534, https://doi.org/10.3390/ijerph19127534, 2022.

Barret, B., Emili, E., and Le Flochmoen, E.: A tropopause-related climatological a priori profile for IASI-SOFRID ozone retrievals: improvements and validation, Atmos. Meas. Tech., 13, 5237–5257, https://doi.org/10.5194/amt-13-5237-2020, 2020 (data available at: https://thredds.sedoo.fr/iasi-sofrid-o3-co/, last access: 15 March 2021).

Bauwens, M., Verreyken, B., Stavrakou, T., Müller, J. F., and Smedt, I. D.: Spaceborne evidence for significant anthropogenic VOC trends in Asian cities over 2005–2019, Environ. Res. Lett., 17, 015008, https://doi.org/10.1088/1748-9326/ac46eb, 2022.

Boynard, A., Hurtmans, D., Koukouli, M. E., Goutail, F., Bureau, J., Safieddine, S., Lerot, C., Hadji-Lazaro, J., Wespes, C., Pommereau, J.-P., Pazmino, A., Zyrichidou, I., Balis, D., Barbe, A., Mikhailenko, S. N., Loyola, D., Valks, P., Van Roozendael, M., Coheur, P.-F., and Clerbaux, C.: Seven years of IASI ozone retrievals from FORLI: validation with independent total column and vertical profile measurements, Atmos. Meas. Tech., 9, 4327–4353, https://doi.org/10.5194/amt-9-4327-2016, 2016.

Boynard, A., Hurtmans, D., Garane, K., Goutail, F., Hadji-Lazaro, J., Koukouli, M. E., Wespes, C., Vigouroux, C., Keppens, A., Pommereau, J.-P., Pazmino, A., Balis, D., Loyola, D., Valks, P., Sussmann, R., Smale, D., Coheur, P.-F., and Clerbaux, C.: Validation of the IASI FORLI/EUMETSAT ozone products using satellite (GOME-2), ground-based (Brewer–Dobson, SAOZ, FTIR) and ozonesonde measurements, Atmos. Meas. Tech., 11, 5125–5152, https://doi.org/10.5194/amt-11-5125-2018, 2018.

Chai, T., Draxler, R., and Stein, A.: Source term estimation using air concentration measurements and a Lagrangian dispersion model – Experiments with pseudo and real cesium-137 observations from the Fukushima nuclear accident, Atmos. Environ., 106, 241-251, https://doi.org/10.1016/j.atmosenv.2015.01.070, 2015.

Chen, S., Wang, W., Li, M., Mao, J., Ma, N., Liu, J., Bai, Z., Zhou, L., Wang, X., Bian, J., and Yu, P.: The Contribution of Local Anthropogenic Emissions to Air Pollutants in Lhasa on the Tibetan Plateau, J. Geophys. Res.-Atmos., 127, e2021JD036202, https://doi.org/10.1029/2021jd036202, 2022a.

Chen, Y., Lin, W., Xu, X., and Zheng, X.: Surface ozone in southeast Tibet: variations and implications of tropospheric

ozone sink over a highland, Environ. Chem., 19, 328–341, https://doi.org/10.1071/EN22015, 2022b.

Chen, Y., Zhou, Y., NixiaCiren, Zhang, H., Wang, C., GesangDeji, and Wang, X.: Spatiotemporal variations of surface ozone and its influencing factors across Tibet: A Geodetector-based study, Sci. Total Environ., 813, 152651, https://doi.org/10.1016/j.scitotenv.2021.152651, 2022c.

Cohen, M. D., Stunder, B. J. B., Rolph, G. D., Draxler, R. R., Stein, A. F., and Ngan, F.: NOAA's HYSPLIT Atmospheric Transport and Dispersion Modeling System, B. Am. Meteorol. Soc., 96, 2059-2077, https://doi.org/10.1175/bams-d-14-00110.1, 2015.

Cooper, O. R., Parrish, D. D., Stohl, A., Trainer, M., Nédélec, P., Thouret, V., Cammas, J. P., Oltmans, S. J., Johnson, B. J., Tarasick, D., Leblanc, T., McDermid, I. S., Jaffe, D., Gao, R., Stith, J., Ryerson, T., Aikin, K., Campos, T., Weinheimer, A., and Avery, M. A.: Increasing springtime ozone mixing ratios in the free troposphere over western North America, Nature, 463, 344–348, https://doi.org/10.1038/nature08708, 2010.

Copernicus Climate Change Service Climate Data Store: Ozone monthly gridded data from 1970 to present derived from satellite observations, Copernicus Climate Change Service (C3S) Climate Data Store (CDS) [data set], https://doi.org/10.24381/cds.4ebfe4eb, 2020.

Cristofanelli, P., Bracci, A., Sprenger, M., Marinoni, A., Bonafè, U., Calzolari, F., Duchi, R., Laj, P., Pichon, J. M., Roccato, F., Venzac, H., Vuillermoz, E., and Bonasoni, P.: Tropospheric ozone variations at the Nepal Climate Observatory-Pyramid (Himalayas, 5079 m a.s.l.) and influence of deep stratospheric intrusion events, Atmos. Chem. Phys., 10, 6537–6549, https://doi.org/10.5194/acp-10-6537-2010, 2010.

Cui, Y., Lin, J., Song, C., Liu, M., Yan, Y., Xu, Y., and Huang, B.: Rapid growth in nitrogen dioxide pollution over Western China, 2005–2013, Atmos. Chem. Phys., 16, 6207–6221, https://doi.org/10.5194/acp-16-6207-2016, 2016.

Cui, Y. Y., Liu, S., Bai, Z., Bian, J., Li, D., Fan, K., McKeen, S. A., Watts, L. A., Ciciora, S. J., and Gao, R.-S.: Religious burning as a potential major source of atmospheric fine aerosols in summertime Lhasa on the Tibetan Plateau, Atmos. Environ., 181, 186–191, https://doi.org/10.1016/j.atmosenv.2018.03.025, 2018.

Desqueyroux, H., Pujet, J. C., Prosper, M., Squinazi, F., and Momas, I.: Short-term effects of low-level air pollution on respiratory health of adults suffering from moderate to severe asthma, Environ. Res., 89, 29–37, https://doi.org/10.1006/enrs.2002.4357, 2002.

Ding, A., Wang, T., and Fu, C.: Transport characteristics and origins of carbon monoxide and ozone in Hong Kong, South China, J. Geophys. Res.-Atmos., 118, 9475–9488, https://doi.org/10.1002/jgrd.50714, 2013.

Ding, T., Gao, H., and Yuan, Y.: The record-breaking northward shift of the western Pacific subtropical high in summer 2018 and the possible role of cross-equatorial flow over the Bay of Bengal, Theor. Appl. Climatol., 139, 701–710, https://doi.org/10.1007/s00704-019-02997-4, 2019.

Dufour, G., Eremenko, M., Griesfeller, A., Barret, B., LeFlochmoën, E., Clerbaux, C., Hadji-Lazaro, J., Coheur, P.-F., and Hurtmans, D.: Validation of three different scientific ozone products retrieved from IASI spectra using ozonesondes, Atmos. Meas. Tech., 5, 611–630, https://doi.org/10.5194/amt-5-611-2012, 2012.

Geng, G., Zhang, Q., Martin, R. V., Lin, J., Huo, H., Zheng, B., Wang, S., and He, K.: Impact of spatial proxies on the representation of bottom-up emission inventories: A satellite-based analysis, Atmos. Chem. Phys., 17, 4131–4145, https://doi.org/10.5194/acp-17-4131-2017, 2017.

Giglio, L., Randerson, J. T., and van der Werf, G. R.: Analysis of daily, monthly, and annual burned area using the fourth-generation global fire emissions database (GFED4), J. Geophys. Res.-Biogeo., 118, 317–328, https://doi.org/10.1002/jgrg.20042, 2013.

Global Modeling and Assimilation Office (GMAO): MERRA-2 tavg1_2d_flx_Nx: 2d,1-Hourly, Time-Averaged, Single-Level, Assimilation, Surface Flux Diagnostics V5.12.4, Goddard Earth Sciences Data and Information Services Center (GES DISC) [data set], Greenbelt, MD, USA, https://doi.org/10.5067/7MCPBJ41Y0K6, 2015a.

Global Modeling and Assimilation Office (GMAO): MERRA-2 tavg1_2d_int_Nx: 2d,1-Hourly, Time-Averaged, Single-Level, Assimilation, Vertically Integrated Diagnostics V5.12.4, Goddard Earth Sciences Data and Information Services Center (GES DISC) [data set], Greenbelt, MD, USA, https://doi.org/10.5067/Q5GVUVUIVGO7, 2015b.

Global Modeling and Assimilation Office (GMAO): MERRA-2 tavg1_2d_slv_Nx: 2d,1-Hourly, Time-Averaged, Single-Level, Assimilation, Single-Level Diagnostics V5.12.4, Goddard Earth Sciences Data and Information Services Center (GES DISC) [data set], Greenbelt, MD, USA, https://doi.org/10.5067/VJAFPLI1CSIV, 2015c.

Global Modeling and Assimilation Office (GMAO): MERRA-2 tavg3_3d_asm_Nv: 3d,3-Hourly, Time-Averaged, Model-Level, Assimilation, Assimilated Meteorological Fields V5.12.4, Goddard Earth Sciences Data and Information Services Center (GES DISC) [data set], Greenbelt, MD, USA, https://doi.org/10.5067/SUOQESM06LPK, 2015d.

Han, H., Zhang, L., Liu, Z., Yue, X., Shu, L., Wang, X., and Zhang, Y.: Narrowing Differences in Urban and Nonurban Surface Ozone in the Northern Hemisphere Over 1990–2020, Environ. Sci. Technol. Lett., 10, 410–417, https://doi.org/10.1021/acs.estlett.3c00105, 2023.

Hu, Y., Yu, H., Kang, S., Yang, J., Chen, X., Yin, X., and Chen, P.: Modeling the transport of PM_{10}, $PM_{2.5}$, and O_3 from South Asia to the Tibetan Plateau, Atmos. Res., 303, 107323, https://doi.org/10.1016/j.atmosres.2024.107323, 2024.

Kalsoom, U., Wang, T., Ma, C., Shu, L., Huang, C., and Gao, L.: Quadrennial variability and trends of surface ozone across China during 2015–2018: A regional approach, Atmos. Environ., 245, 117989, https://doi.org/10.1016/j.atmosenv.2020.117989, 2021.

Kantha, L. H. and Clayson, C. A.: An improved mixed layer model for geophysical applications, J. Geophys. Res.-Oceans, 99, 25235–25266, https://doi.org/10.1029/94jc02257, 2012.

Kim, H. C., Chai, T., Stein, A., and Kondragunta, S.: Inverse modeling of fire emissions constrained by smoke plume transport using HYSPLIT dispersion model and geostationary satellite observations, Atmos. Chem. Phys., 20, 10259–10277, https://doi.org/10.5194/acp-20-10259-2020, 2020.

Kong, H., Lin, J., Zhang, R., Liu, M., Weng, H., Ni, R., Chen, L., Wang, J., Yan, Y., and Zhang, Q.: High-resolution $(0.05° \times 0.05°)$ NO_x emissions in the Yangtze River Delta

inferred from OMI, Atmos. Chem. Phys., 19, 12835–12856, https://doi.org/10.5194/acp-19-12835-2019, 2019.

Kong, H., Lin, J., Chen, L., Zhang, Y., Yan, Y., Liu, M., Ni, R., Liu, Z., and Weng, H.: Considerable Unaccounted Local Sources of NO(x) Emissions in China Revealed from Satellite, Environ. Sci. Technol., 56, 7131–7142, https://doi.org/10.1021/acs.est.1c07723, 2022.

Kong, H., Lin, J., Zhang, Y., Li, C., Xu, C., Shen, L., Liu, X., Yang, K., Su, H., and Xu, W.: High natural nitric oxide emissions from lakes on Tibetan Plateau under rapid warming, Nat. Geosci., 16, 474–477, https://doi.org/10.1038/s41561-023-01200-8, 2023.

Kong, H., Lin, J., Ni, R., Du, M., Wang, J., Chen, L., Xu, C., Yan, Y., Weng, H., and Zhang, Y.: Satellite Detected Weak Decline of Nitrogen Oxides Emissions in Economically Small Cities of China, Environ. Res. Lett., 20, 074046, https://doi.org/10.1088/1748-9326/ade170, 2025.

Li, K., Jacob, D. J., Liao, H., Shen, L., Zhang, Q., and Bates, K. H.: Anthropogenic drivers of 2013–2017 trends in summer surface ozone in China, P. Natl. Acad. Sci. USA, 116, 422–427, https://doi.org/10.1073/pnas.1812168116, 2019.

Li, K., Jacob, D. J., Liao, H., Qiu, Y. L., Shen, L., Zhai, S. X., Bates, K. H., Sulprizio, M. P., Song, S. J., Lu, X., Zhang, Q., Zheng, B., Zhang, Y. L., Zhang, J. Q., Lee, H. C., and Kuk, S. K.: Ozone pollution in the North China Plain spreading into the late-winter haze season, P. Natl. Acad. Sci. USA, 118, 7, https://doi.org/10.1073/pnas.2015797118, 2021a.

Li, M., Liu, H., Geng, G., Hong, C., Liu, F., Song, Y., Tong, D., Zheng, B., Cui, H., Man, H., Zhang, Q., and He, K.: Anthropogenic emission inventories in China: a review, Nat. Sci. Rev., 4, 834–866, https://doi.org/10.1093/nsr/nwx150, 2017.

Li, Q., Gong, D., Wang, H., Deng, S., Zhang, C., Mo, X., Chen, J., and Wang, B.: Tibetan Plateau is vulnerable to aromatic-related photochemical pollution and health threats: A case study in Lhasa, Sci. Total Environ., 904, 166494, https://doi.org/10.1016/j.scitotenv.2023.166494, 2023a.

Li, R., Xu, M., Li, M., Chen, Z., Zhao, N., Gao, B., and Yao, Q.: Identifying the spatiotemporal variations in ozone formation regimes across China from 2005 to 2019 based on polynomial simulation and causality analysis, Atmos. Chem. Phys., 21, 15631–15646, https://doi.org/10.5194/acp-21-15631-2021, 2021b.

Li, W., Han, X., Li, J., Lun, X., and Zhang, M.: Assessment of surface ozone production in Qinghai, China with satellite-constrained VOCs and NO$_x$ emissions, Sci. Total Environ., 905, 166602, https://doi.org/10.1016/j.scitotenv.2023.166602, 2023b.

Lin, J. T. and McElroy, M. B.: Impacts of boundary layer mixing on pollutant vertical profiles in the lower troposphere: Implications to satellite remote sensing, Atmos. Environ., 44, 1726–1739, https://doi.org/10.1016/j.atmosenv.2010.02.009, 2010.

Lin, J.-T., Liu, M.-Y., Xin, J.-Y., Boersma, K. F., Spurr, R., Martin, R., and Zhang, Q.: Influence of aerosols and surface reflectance on satellite NO$_2$ retrieval: seasonal and spatial characteristics and implications for NO$_x$ emission constraints, Atmos. Chem. Phys., 15, 11217–11241, https://doi.org/10.5194/acp-15-11217-2015, 2015a.

Lin, J.-T., Martin, R. V., Boersma, K. F., Sneep, M., Stammes, P., Spurr, R., Wang, P., Van Roozendael, M., Clémer, K., and Irie, H.: Retrieving tropospheric nitrogen dioxide from the Ozone Monitoring Instrument: effects of aerosols, surface reflectance anisotropy, and vertical profile of nitrogen dioxide, Atmos. Chem. Phys., 14, 1441–1461, https://doi.org/10.5194/acp-14-1441-2014, 2014.

Lin, W. L., Xu, X. B., Zheng, X. D., Dawa, J., Baima, C., and Ma, J.: Two-year measurements of surface ozone at Dangxiong, a remote highland site in the Tibetan Plateau, J. Environ. Sci., 31, 133–145, https://doi.org/10.1016/j.jes.2014.10.022, 2015b.

Liu, M., Lin, J., Boersma, K. F., Pinardi, G., Wang, Y., Chimot, J., Wagner, T., Xie, P., Eskes, H., Van Roozendael, M., Hendrick, F., Wang, P., Wang, T., Yan, Y., Chen, L., and Ni, R.: Improved aerosol correction for OMI tropospheric NO$_2$ retrieval over East Asia: constraint from CALIOP aerosol vertical profile, Atmos. Meas. Tech., 12, 1–21, https://doi.org/10.5194/amt-12-1-2019, 2019.

Liu, Y. and Wang, T.: Worsening urban ozone pollution in China from 2013 to 2017 – Part 2: The effects of emission changes and implications for multi-pollutant control, Atmos. Chem. Phys., 20, 6323–6337, https://doi.org/10.5194/acp-20-6323-2020, 2020a.

Liu, Y. and Wang, T.: Worsening urban ozone pollution in China from 2013 to 2017 – Part 1: The complex and varying roles of meteorology, Atmos. Chem. Phys., 20, 6305–6321, https://doi.org/10.5194/acp-20-6305-2020, 2020b.

Liu, Y., Geng, G., Cheng, J., Liu, Y., Xiao, Q., Liu, L., Shi, Q., Tong, D., He, K., and Zhang, Q.: Drivers of Increasing Ozone during the Two Phases of Clean Air Actions in China 2013–2020, Environ. Sci. Technol., 57, 8954–8964, https://doi.org/10.1021/acs.est.3c00054, 2023.

Lu, F., Li, S., Shen, B., Zhang, J., Liu, L., Shen, X., and Zhao, R.: The emission characteristic of VOCs and the toxicity of BTEX from different mosquito-repellent incenses, J. Hazard. Mater., 384, 121428, https://doi.org/10.1016/j.jhazmat.2019.121428, 2020a.

Lu, X., Hong, J., Zhang, L., Cooper, O. R., Schultz, M. G., Xu, X., Wang, T., Gao, M., Zhao, Y., and Zhang, Y.: Severe Surface Ozone Pollution in China: A Global Perspective, Environ. Sci. Technol. Lett., 5, 487–494, https://doi.org/10.1021/acs.estlett.8b00366, 2018.

Lu, X., Zhang, L., Chen, Y., Zhou, M., Zheng, B., Li, K., Liu, Y., Lin, J., Fu, T.-M., and Zhang, Q.: Exploring 2016–2017 surface ozone pollution over China: source contributions and meteorological influences, Atmos. Chem. Phys., 19, 8339–8361, https://doi.org/10.5194/acp-19-8339-2019, 2019.

Lu, X., Zhang, L., Wang, X., Gao, M., Li, K., Zhang, Y., Yue, X., and Zhang, Y.: Rapid Increases in Warm-Season Surface Ozone and Resulting Health Impact in China Since 2013, Environ. Sci. Technol. Lett., 7, 240–247, https://doi.org/10.1021/acs.estlett.0c00171, 2020b.

Ma, J., Lin, W. L., Zheng, X. D., Xu, X. B., Li, Z., and Yang, L. L.: Influence of air mass downward transport on the variability of surface ozone at Xianggelila Regional Atmosphere Background Station, southwest China, Atmos. Chem. Phys., 14, 5311–5325, https://doi.org/10.5194/acp-14-5311-2014, 2014.

Ma, J., Zhou, X., Xu, X., Xu, X., Gromov, S., and Lelieveld, J.: Chapter 15 – Ozone and aerosols over the Tibetan Plateau, in: Asian Atmospheric Pollution, edited by: Singh, R. P., Elsevier, 287–302, https://doi.org/10.1016/B978-0-12-816693-2.00008-1, 2022.

Marinoni, A., Cristofanelli, P., Laj, P., Duchi, R., Putero, D., Calzolari, F., Landi, T. C., Vuillermoz, E., Maione, M., and Bonasoni, P.: High black carbon and ozone concentrations during pollution transport in the Himalayas: Five years of continuous observations at NCO-P global GAW station, J. Environ. Sci., 25, 1618–1625, https://doi.org/10.1016/s1001-0742(12)60242-3, 2013.

Matricardi, M., Chevallier, F., Kelly, G., and Thépaut, J.-N.: An improved general fast radiative transfer model for the assimilation of radiance observations, Quarterly Journal of the Royal Meteorological Society, 130, 153–173, https://doi.org/10.1256/qj.02.181, 2004.

Mauzerall, D. L. and Wang, X.: PROTECTING AGRICULTURAL CROPS FROM THE EFFECTS OF TROPOSPHERIC OZONE EXPOSURE: Reconciling Science and Standard Setting in the United States, Europe, and Asia, Annu. Rev. Energ. Env., 26, 237–268, https://doi.org/10.1146/annurev.energy.26.1.237, 2001.

Miles, G. M., Siddans, R., Kerridge, B. J., Latter, B. G., and Richards, N. A. D.: Tropospheric ozone and ozone profiles retrieved from GOME-2 and their validation, Atmos. Meas. Tech., 8, 385–398, https://doi.org/10.5194/amt-8-385-2015, 2015.

Ni, R., Lin, J., Yan, Y., and Lin, W.: Foreign and domestic contributions to springtime ozone over China, Atmos. Chem. Phys., 18, 11447–11469, https://doi.org/10.5194/acp-18-11447-2018, 2018.

Ni, Y., Yang, Y., Wang, H., Li, H., Li, M., Wang, P., Li, K., and Liao, H.: Contrasting changes in ozone during 2019–2021 between eastern and the other regions of China attributed to anthropogenic emissions and meteorological conditions, Sci. Total Environ., 908, 168272, https://doi.org/10.1016/j.scitotenv.2023.168272, 2024.

O'Rourke, P. R., Smith, S. J., Mott, A., Ahsan, H., McDuffie, E. E., Crippa, M., Klimont, S., McDonald, B., Wang, Z., Nicholson, M. B., Feng, L., and Hoesly, R. M.: CEDS v-2021-02-05 Emission Data 1975–2019 (Feb-05-2021), Zenodo [data set], https://doi.org/10.5281/zenodo.4509372, 2021.

Pan, W., Gong, S., Lu, K., Zhang, L., Xie, S., Liu, Y., Ke, H., Zhang, X., and Zhang, Y.: Multi-scale analysis of the impacts of meteorology and emissions on PM$_{2.5}$ and O$_3$ trends at various regions in China from 2013 to 2020 3. Mechanism assessment of O$_3$ trends by a model, Sci. Total Environ., 857, 159592, https://doi.org/10.1016/j.scitotenv.2022.159592, 2023.

Putero, D., Landi, T. C., Cristofanelli, P., Marinoni, A., Laj, P., Duchi, R., Calzolari, F., Verza, G. P., and Bonasoni, P.: Influence of open vegetation fires on black carbon and ozone variability in the southern Himalayas (NCO-P, 5079 m a.s.l.), Environ. Pollut., 184, 597–604, https://doi.org/10.1016/j.envpol.2013.09.035, 2014.

Ran, L., Lin, W. L., Deji, Y. Z., La, B., Tsering, P. M., Xu, X. B., and Wang, W.: Surface gas pollutants in Lhasa, a highland city of Tibet – current levels and pollution implications, Atmos. Chem. Phys., 14, 10721–10730, https://doi.org/10.5194/acp-14-10721-2014, 2014.

Stein, A. F., Draxler, R. R., Rolph, G. D., Stunder, B. J. B., Cohen, M. D., and Ngan, F.: NOAA's HYSPLIT Atmospheric Transport and Dispersion Modeling System, B. Am. Meteorol. Soc., 96, 2059–2077, https://doi.org/10.1175/BAMS-D-14-00110.1, 2015.

Stohl, A.: A backward modeling study of intercontinental pollution transport using aircraft measurements, J. Geophys. Res., 108, 4370, https://doi.org/10.1029/2002jd002862, 2003

Tan, W., Wang, H., Su, J., Sun, R., He, C., Lu, X., Lin, J., Xue, C., Wang, H., Liu, Y., Liu, L., Zhang, L., Wu, D., Mu, Y., and Fan, S.: Soil Emissions of Reactive Nitrogen Accelerate Summertime Surface Ozone Increases in the North China Plain, Environ. Sci. Technol., 57, 12782–12793, https://doi.org/10.1021/acs.est.3c01823, 2023.

Tang, G., Yao, D., Kang, Y., Liu, Y., Liu, Y., Wang, Y., Bai, Z., Sun, J., Cong, Z., Xin, J., Liu, Z., Zhu, Z., Geng, Y., Wang, L., Li, T., Li, X., Bian, J., and Wang, Y.: The urgent need to control volatile organic compound pollution over the Qinghai-Tibet Plateau, iScience, 25, 105688, https://doi.org/10.1016/j.isci.2022.105688, 2022.

Wang, J., Ge, B., and Wang, Z.: Ozone Production Efficiency in Highly Polluted Environments, Current Pollution Reports, 4, 198–207, https://doi.org/10.1007/s40726-018-0093-9, 2018.

Wang, M., Chen, X., Jiang, Z., He, T.-L., Jones, D., Liu, J., and Shen, Y.: Meteorological and anthropogenic drivers of surface ozone change in the North China Plain in 2015–2021, Sci. Total Environ., 906, 167763, https://doi.org/10.1016/j.scitotenv.2023.167763, 2024.

Wang, T., Dai, J., Lam, K. S., Nan Poon, C., and Brasseur, G. P.: Twenty-Five Years of Lower Tropospheric Ozone Observations in Tropical East Asia: The Influence of Emissions and Weather Patterns, Geophys. Res. Lett., 46, 11463–11470, https://doi.org/10.1029/2019gl084459, 2019.

Wang, W., van der A, R., Ding, J., van Weele, M., and Cheng, T.: Spatial and temporal changes of the ozone sensitivity in China based on satellite and ground-based observations, Atmos. Chem. Phys., 21, 7253–7269, https://doi.org/10.5194/acp-21-7253-2021, 2021.

Warneck, P.: Chemistry of the Natural Atmosphere, 2nd Edn., Academic Press, https://www.sciencedirect.com/bookseries/international-geophysics/vol/71/suppl/C (last access: 15 January 2025), 1999.

Weng, H., Lin, J., Martin, R., Millet, D. B., Jaeglé, L., Ridley, D., Keller, C., Li, C., Du, M., and Meng, J.: Global high-resolution emissions of soil NO$_x$, sea salt aerosols, and biogenic volatile organic compounds, Sci. Data, 7, 148, https://doi.org/10.1038/s41597-020-0488-5, 2020.

Weng, X., Forster, G. L., and Nowack, P.: A machine learning approach to quantify meteorological drivers of ozone pollution in China from 2015 to 2019, Atmos. Chem. Phys., 22, 8385–8402, https://doi.org/10.5194/acp-22-8385-2022, 2022.

WHO: Review of evidence on health aspects of air pollution: REVIHAAP project: technical report, World Health Organization, Regional Office for Europe, https://iris.who.int/handle/10665/341712 (last access: 20 January 2025), 2013.

Wu, S., Mickley, L. J., Jacob, D. J., Logan, J. A., Yantosca, R. M., and Rind, D.: Why are there large differences between models in global budgets of tropospheric ozone?, J. Geophys. Res.-Atmos., 112, D05302, https://doi.org/10.1029/2006jd007801, 2007.

Xu, H., Yu, H., Xu, B., Wang, Z., Wang, F., Wei, Y., Liang, W., Liu, J., Liang, D., Feng, Y., and Shi, G.: Machine learning coupled structure mining method visualizes the impact of multiple drivers on ambient ozone, Commun. Earth Environ., 4, 265, https://doi.org/10.1038/s43247-023-00932-0, 2023.

Xu, W., Lin, W., Xu, X., Tang, J., Huang, J., Wu, H., and Zhang, X.: Long-term trends of surface ozone and its influencing factors at the Mt Waliguan GAW station, China – Part 1: Overall trends and characteristics, Atmos. Chem. Phys., 16, 6191–6205, https://doi.org/10.5194/acp-16-6191-2016, 2016.

Xu, W., Xu, X., Lin, M., Lin, W., Tarasick, D., Tang, J., Ma, J., and Zheng, X.: Long-term trends of surface ozone and its influencing factors at the Mt Waliguan GAW station, China – Part 2: The roles of anthropogenic emissions and climate variability, Atmos. Chem. Phys., 18, 773–798, https://doi.org/10.5194/acp-18-773-2018, 2018a.

Xu, X., Zhang, H., Lin, W., Wang, Y., Xu, W., and Jia, S.: First simultaneous measurements of peroxyacetyl nitrate (PAN) and ozone at Nam Co in the central Tibetan Plateau: impacts from the PBL evolution and transport processes, Atmos. Chem. Phys., 18, 5199–5217, https://doi.org/10.5194/acp-18-5199-2018, 2018b.

Xu, X., Lin, W., Xu, W., Jin, J., Wang, Y., Zhang, G., Zhang, X., Ma, Z., Dong, Y., Ma, Q., Yu, D., Li, Z., Wang, D., and Zhao, H.: Long-term changes of regional ozone in China: implications for human health and ecosystem impacts, Elementa: Science of the Anthropocene, 8, 13, https://doi.org/10.1525/elementa.409, 2020 (data available at: https://igacproject.org/activities/TOAR, last access: 21 April 2024).

Xue, L. K., Wang, T., Zhang, J. M., Zhang, X. C., Deliger, Poon, C. N., Ding, A. J., Zhou, X. H., Wu, W. S., Tang, J., Zhang, Q. Z., and Wang, W. X.: Source of surface ozone and reactive nitrogen speciation at Mount Waliguan in western China: New insights from the 2006 summer study, J. Geophys. Res., 116, D07306, https://doi.org/10.1029/2010jd014735, 2011.

Yan, Y., Lin, J., Chen, J., and Hu, L.: Improved simulation of tropospheric ozone by a global-multi-regional two-way coupling model system, Atmos. Chem. Phys., 16, 2381–2400, https://doi.org/10.5194/acp-16-2381-2016, 2016.

Yan, Y., Lin, J., and He, C.: Ozone trends over the United States at different times of day, Atmos. Chem. Phys., 18, 1185–1202, https://doi.org/10.5194/acp-18-1185-2018, 2018a.

Yan, Y., Pozzer, A., Ojha, N., Lin, J., and Lelieveld, J.: Analysis of European ozone trends in the period 1995–2014, Atmos. Chem. Phys., 18, 5589–5605, https://doi.org/10.5194/acp-18-5589-2018, 2018b.

Yang, J., Kang, S., Hu, Y., Chen, X., and Rai, M.: Influence of South Asian Biomass Burning on Ozone and Aerosol Concentrations Over the Tibetan Plateau, Adv. Atmos. Sci., 39, 1184–1197, https://doi.org/10.1007/s00376-022-1197-0, 2022.

Ye, X., Zhang, L., Wang, X., Lu, X., Jiang, Z., Lu, N., Li, D., and Xu, J.: Spatial and temporal variations of surface background ozone in China analyzed with the grid-stretching capability of GEOS-Chem High Performance, Sci. Total Environ., 914, 169909, https://doi.org/10.1016/j.scitotenv.2024.169909, 2024.

Yin, H., Sun, Y., Notholt, J., Palm, M., Ye, C., and Liu, C.: Quantifying the drivers of surface ozone anomalies in the urban areas over the Qinghai-Tibet Plateau, Atmos. Chem. Phys., 22, 14401–14419, https://doi.org/10.5194/acp-22-14401-2022, 2022.

Yin, X., Kang, S., de Foy, B., Cong, Z., Luo, J., Zhang, L., Ma, Y., Zhang, G., Rupakheti, D., and Zhang, Q.: Surface ozone at Nam Co in the inland Tibetan Plateau: variation, synthesis comparison and regional representativeness, Atmos. Chem. Phys., 17, 11293–11311, https://doi.org/10.5194/acp-17-11293-2017, 2017.

Yuan, Y., Gao, H., and Ding, T.: The extremely north position of the western Pacific subtropical high in summer of 2018: Important role of the convective activities in the western Pacific, Int. J. Climatol., 40, 1361–1374, https://doi.org/10.1002/joc.6274, 2019.

Zhang, M., Wang, S., Yu, W., Tao, C., Zhu, S., Ma, J., Wang, P., and Zhang, H.: The Major Role of Anthropogenic Emission Underestimation in PM2.5 Estimation Uncertainty Over the Tibetan Plateau, 52, e2024GL110513, https://doi.org/10.1029/2024GL110513, 2025.

Zhang, Y., Lin, J., Liu, M., Kong, H., Chen, L., Weng, H., and Li, C.: High-resolution Tropospheric NO_2 Retrieval over Asia based on OMI POMINO v2.1 and quantitative comparison with other products, National Remote Sensing Bulletin, 26, 971–987, https://doi.org/10.11834/jrs.20221413, 2022.

Zhao, H., Li, X., Zhang, Q., Jiang, X., Lin, J., Peters, G. P., Li, M., Geng, G., Zheng, B., Huo, H., Zhang, L., Wang, H., Davis, S. J., and He, K.: Effects of atmospheric transport and trade on air pollution mortality in China, Atmos. Chem. Phys., 17, 10367–10381, https://doi.org/10.5194/acp-17-10367-2017, 2017.

Zheng, B., Tong, D., Li, M., Liu, F., Hong, C., Geng, G., Li, H., Li, X., Peng, L., Qi, J., Yan, L., Zhang, Y., Zhao, H., Zheng, Y., He, K., and Zhang, Q.: Trends in China's anthropogenic emissions since 2010 as the consequence of clean air actions, Atmos. Chem. Phys., 18, 14095–14111, https://doi.org/10.5194/acp-18-14095-2018, 2018.

Zheng, D. and Shi, M.: Multiple environmental policies and pollution haven hypothesis: Evidence from China's polluting industries, J. Clean. Prod., 141, 295–304, https://doi.org/10.1016/j.jclepro.2016.09.091, 2017.

Zheng, H., Kong, S., He, Y., Song, C., Cheng, Y., Yao, L., Chen, N., and Zhu, B.: Enhanced ozone pollution in the summer of 2022 in China: The roles of meteorology and emission variations, Atmos. Environ., 301, 119701, https://doi.org/10.1016/j.atmosenv.2023.119701, 2023.

Zhu, T., Lin, W., Song, Y., Cai, X., Zou, H., Kang, L., Zhou, L., and Akimoto, H.: Downward transport of ozone-rich air near Mt. Everest, Geophys. Res. Lett., 33, L23809, https://doi.org/10.1029/2006gl027726, 2006.

Ziemke, J. R., Chandra, S., and Bhartia, P. K.: "Cloud slicing": A new technique to derive upper tropospheric ozone from satellite measurements, J. Geophys. Res.-Atmos., 106, 9853–9867, https://doi.org/10.1029/2000JD900768, 2001.

Ziemke, J. R., Chandra, S., Duncan, B. N., Froidevaux, L., Bhartia, P. K., Levelt, P. F., and Waters, J. W.: Tropospheric ozone determined from Aura OMI and MLS: Evaluation of measurements and comparison with the Global Modeling Initiative's Chemical Transport Model, J. Geophys. Res., 111, D19303, https://doi.org/10.1029/2006jd007089, 2006.

Ziemke, J. R., Chandra, S., Labow, G. J., Bhartia, P. K., Froidevaux, L., and Witte, J. C.: A global climatology of tropospheric and stratospheric ozone derived from Aura OMI and MLS measurements, Atmos. Chem. Phys., 11, 9237–9251, https://doi.org/10.5194/acp-11-9237-2011, 2011 (data available at: https://acd-ext.gsfc.nasa.gov/Data_services/cloud_slice/new_data.html, last access: 21 April 2024).